



Decreased *miR-940* expression can predict a negative prognosis in early-stage nonsmoking female lung adenocarcinoma

Qianli Ma^{1^}, Jin Zhang¹, Jingjing Huang¹, Xiaowei Wang², Fei Xiao¹, Huajie Xing¹, Ye Wang², Yongqing Guo¹, Bin Shi¹, Zhiyi Song¹, Deruo Liu¹, Chaozeng Si³, Hidehito Horinouchi⁴, Chaoyang Liang¹

¹Department of Thoracic Surgery, China-Japan Friendship Hospital, Beijing, China; ²Department of Pathology, China-Japan Friendship Hospital, Beijing, China; ³Department of Information Management, China-Japan Friendship Hospital, Beijing, China; ⁴Department of Thoracic Oncology, National Cancer Center Hospital, Tokyo, Japan

Contributions: (I) Conception and design: Q Ma, C Si; (II) Administrative support: D Liu, C Liang; (III) Provision of study materials or patients: Q Ma, J Huang, F Xiao, H Xing; (IV) Collection and assembly of data: Q Ma, X Wang, Y Wang; (V) Data analysis and interpretation: Q Ma, C Si, J Zhang; (VI) Manuscript writing: All authors; (VII) Final approval of manuscript: All authors.

Correspondence to: Deruo Liu. Department of Thoracic Surgery, China-Japan Friendship Hospital, 2 Yinghua East Road, Chaoyang, Beijing 100029, China. Email: deruoliu@vip.sina.com; Chaozeng Si. Department of Information Management, China-Japan Friendship Hospital, 2 Yinghua East Road, Chaoyang, Beijing 100029, China. Email: sichaozeng@163.com; Chaoyang Liang. Department of Thoracic Surgery, China-Japan Friendship Hospital, 2 Yinghua East Road, Chaoyang, Beijing 100029, China. Email: chaoyangliang8@hotmail.com.

Background: Early-stage female lung adenocarcinoma is the most common type of lung cancer encountered in thoracic surgery departments. Tumor-node-metastasis (TNM) staging does not adequately explain a significant stratification phenomenon in the prognosis of patients with stage I lung adenocarcinoma. We aimed to investigate the contributory role of *miR-940* in the prognosis prediction.

Methods: We analyzed the microRNA (miRNA) expression level in tumor tissues (high-risk group *vs.* low-risk group) from 12 non-smoking female patients with stage I lung adenocarcinoma using miRNA array. Bioinformatic analyses of *miR-940* were also carried out based on the public database. Then, quantitative reverse-transcription polymerase chain reaction (qRT-PCR) tests of the tissue samples were further validated. And *miR-940*'s function was analyzed and potential target genes were predicted.

Results: In all, 24 miRNAs were found to be significantly different between the high-risk group and low-risk group. The expression level of *miR-940* was lower in tumor tissue ($P=0.011$), and the survival rate in the high *miR-940* group was higher [hazard ratio (HR) =0.688; $P=0.011$]. Gene Ontology (GO) analysis showed that the assembly functions of targets regulated by *miR-940* were mainly enriched in regulation of myeloid cell differentiation, G1/S transition of mitotic cell cycle, and cellular response to environmental stimulus. *miR-940* is involved in transforming growth factor-beta (TGF-beta) signaling pathway; TNF signaling pathway; and estrogen signaling pathway. The number of lung adenocarcinoma cells (A549) was significantly decreased after *miR-940* was transfected. Ten epithelial-to-mesenchymal-transition (EMT)-associated genes (*MMP9*, *ZEB1*, *CDH1*, *KRT8*, *KRT18*, *KET19*, *TWIST1*, *VIM*, *SNAI1*, and *SNAI2*) were found to be significantly related to *miR-940*.

Conclusions: The present study showed that *miR-940* might be a protective factor for positive prognosis in early stage nonsmoking female lung adenocarcinoma, with transforming growth factor-beta (TGF-beta) pathway, TNF pathway, and matrix metalloprotein (*MMP9*) being potential targets.

Keywords: MicroRNA (miRNA); lung adenocarcinoma; early stage; prognosis; gene expression profile; bioinformatics analysis

Submitted Aug 26, 2021. Accepted for publication Nov 25, 2021.

doi: 10.21037/tlcr-21-906

View this article at: <https://dx.doi.org/10.21037/tlcr-21-906>

[^] ORCID: 0000-0003-2195-8181.

Introduction

Lung cancer is a disease that is a serious threat to human health and has a global range. Epidemiologic reports of malignant tumors (1-3) indicate that morbidity and mortality associated with lung cancer rank first among cancers. Non-small cell lung cancer (NSCLC) is the most common histologic type of lung cancer, accounting for 80–85% of lung cancers in the patient population, with lung adenocarcinoma accounting for the majority of cases (4). Tumor-node-metastasis (TNM) staging is carried out according to the size of the primary tumor, lymph node metastasis status, and distant metastases. TNM staging has taken a central role in the treatment of lung cancer (5). However, the results of recent clinical studies have indicated that TNM staging cannot explain a significant stratification phenomenon in the prognosis of patients with early-stage lung adenocarcinoma (6,7).

MicroRNA (miRNA) is a small, single-stranded, noncoding RNA with a length of 18–25 nucleotides and has a high degree of genetic stability. miRNA degrades messenger RNA (mRNA) or inhibits its translation mainly by combining with the 3' untranslated regions (3'UTR) of the target gene of mRNA, thus resulting in posttranscriptional regulation of gene expression (8). As of August 2012, a total of 2024 kinds of human miRNAs have been included in Sanger miRBase (version 19.0). It is expected that miRNA is involved in the regulation of nearly two-thirds of human protein-coding genes (9). miRNAs play important roles in cell proliferation, differentiation, apoptosis, and individual development. In recent years, studies involving the relationships between miRNA and the occurrence, metastasis, and invasiveness of tumors have become the focus of intense research interest. It has been reported that miRNA abnormalities are closely associated with the occurrence and development of NSCLC (10-14). Recent studies have found miR-940 to be a biomarker in breast cancer (15), thyroid carcinoma (16), and NSCLC (17,18).

Studies concerning the role of miRNA in stage I nonsmoking female lung adenocarcinoma with different prognostic stratifications are rare. We thus endeavored to examine the characteristics of miRNA expression profiles and clarify the potential mechanism mediated by *miR-940*. We present the following article in accordance with the REMARK reporting checklist (available at <https://dx.doi.org/10.21037/tlcr-21-906>).

Methods

Patient specimens

Twenty-eight formalin fixed paraffin embedded samples from female nonsmoking patients with stage I lung adenocarcinoma undergoing surgery in the China-Japan Friendship Hospital between May 2014 and October 2015 were selected (median age 63 years; age range 53–71 years): 6 samples from the high-risk group and 6 samples from the low-risk group were used for analysis of miRNA expression profiles. High and low-risk group were defined by the final survival status. The overall survival time in high-risk group was less than 5 years. While the overall survival time in low-risk group was more than 5 years. Subsequently, 8 samples from the high-risk group and 8 samples from the low-risk group were used for experimental validation of miRNA expression. All specimens were fixed in 4% neutral formalin and embedded in paraffin. And all patients received no more adjuvant treatment. All procedures performed in this study involving human participants were in accordance with the Declaration of Helsinki (as revised in 2013). The study was approved by ethics board of China-Japan Friendship Hospital (No. 2020-116-K75) and informed consent was taken from all the patients.

Cluster analysis

The methods of Euclidean distance function and average linking clustering were applied. Cluster-view 3.0 software was used to carry out clustering analysis for comparative threshold cycle (Ct) values of 24 miRNAs with significant expression differences in 6 patients from the high-risk group and 6 patients from the low-risk group. The expression level of these 24 miRNAs were significant different.

Target selection and analysis

miRanda (MicroRNA.Org/microrna/homedo) (9) and Target Scan (<http://www.Targetscan.Org/>) (19) were used to carry out target prediction. *miR-940* was selected as the target with the most significant difference. The expression level of *miR-940* was analyzed by using the Gene Expression Omnibus (GEO) data from GSE 36681. Meanwhile, the survival rate between the high and low *miR-940* expression groups was compared in The Cancer Genome Atlas (TCGA).

Bioinformatic analysis

Protein-protein interaction (PPI) network, Gene Ontology (GO) term enrichment, and Kyoto Encyclopedia of Genes and Genomes (KEGG) pathway analysis were constructed to reveal the hub genes of the potential target genes on search tool for recurring instances of neighbouring genes (STRING), a web portal for undermining the integrated function of multiple genes (14). Two intersected targets predicated by target prediction software were taken to study the distribution status in the GO database, and the functional embodiments of targets of *miR-940* were clarified (20,21). Fisher's exact test and χ^2 test were mainly used to obtain P and false discovery rate (Fisher's discriminant ratio, FDR) values, respectively, (false-positive rate and re-estimation of P value precision). Based on P value <0.05 and FDR <0.05, significant functions of targets were selected. Pathway classification of *miR-940* was carried out according to KEGG public databases, and significance analysis of targets based on the discrete distribution was carried out to obtain pathway classification of significance (22,23). Fisher's exact test and a chi-square test were mainly used. A P value <0.05 and FDR <0.05 were also the basis to select significant signal transduction pathways wherein the targets participated.

Reverse transcription-quantitative polymerase chain reaction validation

The expression levels of *miR-940* in both high-risk and low-risk groups (8 vs. 8 samples) were analyzed. Total RNA was extracted using miRNeasy FFPE kit (Qiagen Company) according to the manufacturer's instructions. The primer for reverse transcription was *miR-940* (MegaplexIII RT Primers, AB Company), which was conducted with TaqMan MicroRNA Reverse Transcription Kit (AB Company) with U6 small nuclear RNA (snRNA) being used as the internal reference. Three duplicate wells were made for each reaction. The amplification was performed using a quantitative polymerase chain reaction (qPCR) instrument (ABI7500, Applied Biosystems Company, USA). The fold change of each tumor sample relative to the normal sample was calculated using the $2^{-\Delta\Delta C_t}$ method as follows: $[\Delta\Delta C_t = \Delta C_t \text{ experimental group} - \Delta C_t \text{ control group} = (C_t \text{ experimental group miRNA} - C_t \text{ experimental group U6}) - (C_t \text{ control group miRNA} - C_t \text{ control group U6})]$ (24). The fold change $I \geq 2$ indicated that the expression level of miRNA was increased, while the fold change $I < 0.5$ indicated that the expression level of miRNA was decreased.

If the fold change ranged between 0.5 and 2.0, it indicated that there was no change in the expression level of miRNA.

Functional analysis

Cell migration, proliferation, and cell cycle analysis was carried out in lung adenocarcinoma cells (A549). Epithelial-to-mesenchymal-transition (EMT)-associated gene analysis and target genes were predicted by the Kaplan-Meier plotter method.

Cell cycle analysis

DAPI is a fluorescent dye that penetrates the cell membrane and binds to AT in the small bend of the double stranded DNA double helix in the nucleus through Acumen. eX3 high intensity screening platform uses 405nm laser to excite DAPI to produce blue fluorescence. The content of DNA in each phase of the cell cycle is different. Normally, normal cells have the DNA content of diploid cells is 2N in G1 phase. The DNA content of tetraploid cells is 4N in G2/M phase. While the DNA content of S stage is between diploid and tetraploid. DAPI fluorescence intensity is proportional to the DAPI incorporation amount and the amount of DNA in the cells. The DNA amount can be determined by using Acumen's fully automated high-throughput analysis/screening platform after DAPI staining. The percentage of G1, S, G2/M phase cells was calculated to show the cell cycle distribution.

Statistical analysis

The test results of TaqMan miRNA Array were analyzed by *t*-test using the random variance model (RVM) based on a small sample (25). A P value <0.05 and FDR <0.05 indicated a statistically significant difference. The difference in miRNA expression profiles obtained from quantitative RT-PCR (qRT-PCR) was analyzed using SPSS19.0 software (IBM Corporation, Armonk, NY, USA) and independent 2-sample *t*-test.

Results

Experimental

Clinical characters of the 12 patients for miRNA chip

Table 1 Clinical pathological characters of the 12 patients involved in miRNA chip analysis

Group	Age	Gender	Smoke	Location	Size (cm)	Inv.	Subtypes (%)					Stage	Time	Outcome
							L	A	P	MP	S			
B1	60	F	N	LU	2.7	PI+	0	89	10	1	0	IB	36	D
B2	58	F	N	RU	4.0	–	85	5	10	0	0	IB	9	D
B3	65	F	N	RU	1.5	V+	7	50	0	3	40	IA	10	D
B4	68	F	N	LU	4.0	–	5	80	10	5	0	IB	17	D
B5	53	F	N	LL	2.0	–	0	70	30	0	0	IA	96	S
B6	70	F	N	RL	3.0	V+	0	0	2	3	95	IA	8	D
A1	59	F	N	RU	3.0	–	95	5	0	0	0	IA	192	S
A2	62	F	N	RM	3.0	–	5	85	10	0	0	IA	98	D
A3	60	F	N	RL	4.0	–	15	50	35	0	0	IB	180	S
A4	71	F	N	RU	2.0	–	15	85	0	0	0	IA	96	D
A5	66	F	N	LU	2.5	–	80	20	0	0	0	IA	70	S
A6	63	F	N	RU	2.0	–	95	5	0	0	0	IA	156	S

B1–B6: high-risk group; A1–A6: low-risk group. F, female; N, none; LU, left upper lobe; LL, left lower lobe; RM, right middle lobe; RU, right upper lobe; RL, right lower lobe; cm, centimeter; Inv., invasive; PI+, pleural invasion; V+, vessel invasion; L, lepidic subtype; A, acinar subtype; P, papillary subtype; MP, micropapillary subtype; S, solid subtype; D, dead; S, survival.

analysis are shown in *Table 1*. They were all female nonsmoking stage I lung adenocarcinoma patients with a mean age of 62.92 years (SD 5.32 cm; high-risk group: 70.00±6.47; low-risk group: 63.50±4.42; $P=0.0088$). Locations of the lesion were distributed as follows: 3 cases in the left upper lobe, 5 cases in the right upper lobe, 1 case in the left lower lobe, 2 cases in the right lower lobe, and 1 case in the right middle lobe. The size of the tumors was 2.81 cm (SD 0.86 cm; high-risk group: 2.87±1.02; low-risk group: 2.75±0.76; $P=0.7469$). There was 1 case of pleural invasion, 2 cases of vessel invasion in the high-risk group, and no cases of pleural or vessel invasion in the low-risk group. The percentage of the lepidic subtype in the high-risk group and low-risk group was 16.70% and 50.83%, respectively ($P=0.1540$). The percentage of the acinar subtype in the high-risk group and low-risk group was 49.00% and 41.67% ($P=0.7441$), respectively. The percentage of the papillary subtype in the high-risk group and low-risk group was 10.33% and 7.50% ($P=0.7018$), respectively. The percentage of the micropapillary subtype in the high-risk group and low-risk group was 2.00% and 0.00% ($P=0.0343$), respectively. The percentage of the solid subtype in the high-risk group and low-risk group was 22.50% and 0.00% ($P=0.1875$), respectively. The percentage of stage IA in the high-risk and low-risk group

was 50% and 83.33% ($P=0.2596$), respectively.

Survival analysis

The Kaplan-Meier curves of overall survival (OS) indicated that the high-risk (Group A) had shorter OS than did the low-risk (Group B) ($P=0.011$; *Figure 1A*). The cluster figure for 24 types of miRNA in lung adenocarcinoma miRNA expression profiles showed a significant difference between the high-risk group and low-risk group (*Figure 1B*). As can be seen in *Figure S1*, the horizontal axis was the main miRNA cluster; *miR-4293*, *miR-3915*, and *miR-4476* were up-regulated in the high-risk group, while *let-7b-5p*, *miR-197-3p*, *miR-513a-5p*, *miR-940*, *miR-3620-3p*, *miR-3679-3p*, *miR-4484*, *miR-4510*, *miR-4635*, *miR-4640-3p*, *miR-4653-3p*, *miR-4695-3p*, *miR-5195-5p*, *miR-6511b-3p*, *miR-6784-3p*, *miR-6792-3p*, *miR-6793-3p*, *miR-6798-3p*, *miR-6803-3p*, *miR-6805-3p*, and *miR-6862-3p* were downregulated in the high-risk group ($P<0.05$ and $FDR<0.05$).

Bioinformatics

The differential expression of *miR-940* was analyzed by using the GEO data from GSE 36681. The expression level of *miR-940* in the tumor group ($n=56$) was lower than that of the

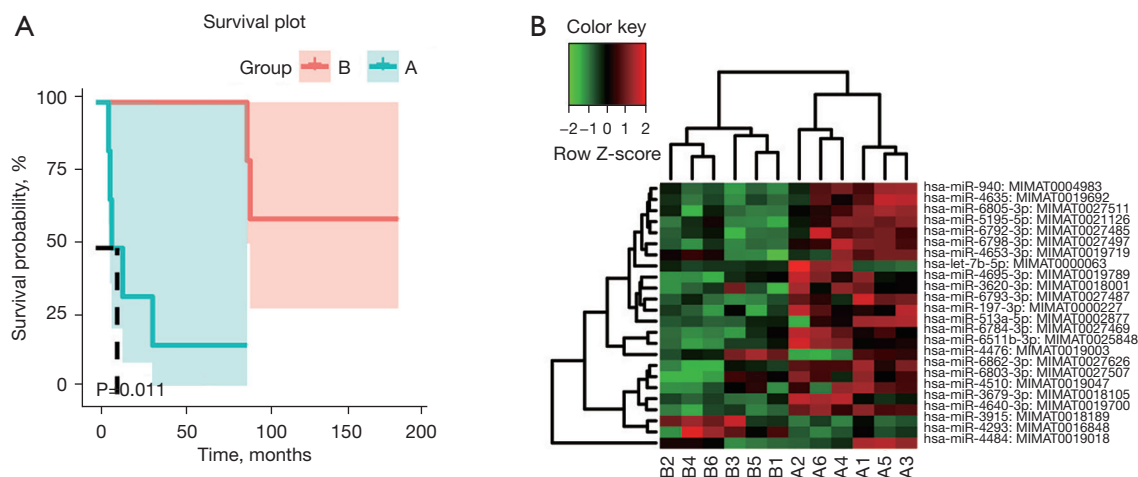


Figure 1 Survival analysis and miRNA chip analysis. (A) Kaplan-Meier curves of overall survival (OS) in the high-risk group and low risk-group from the clinical database. High-risk group (Group A) had shorter OS than did the low-risk group (Group B) ($P=0.011$). (B) The cluster figure for 24 types of miRNA in lung adenocarcinoma miRNA expression profiles that were significantly different between the high-risk group (B1, B2, B3, B4, B5, B6) and low-risk group (A1, A2, A3, A4, A5, A6).

normal tissue ($n=56$; $P=0.013$; *Figure 2A*). The survival rate in the high *miR-940* expression group ($n=253$) was higher than that in the low *miR-940* expression group ($n=252$) in TCGA data [hazard ratio (HR) =0.688; $P=0.011$; *Figure 2B*]. Fourteen upregulated genes [*MYC* (myelocytomatosis), *MAX*, *ELF1* (E74 like ETS transcription factor 1), *CREB1* (cAMP responsive element binding protein 1), *BRD4* (bromodomain containing 4), *CEBPB* [CCAAT/enhancer binding protein (C/EBP), beta], *E2F6* (E2F transcription factor 6), *GABPA* (GA repeat binding protein, alpha), *MAZ* (MYC-associated zinc finger protein), *REST* (RE1-silencing transcription factor), *SPI* (trans-acting transcription factor 1), *YY1* (YY1 transcription factor), *TAF1* (TATA-box binding protein associated factor 1), *SIX5* (sine oculis-related homeobox 5)] were found to be interactional in the PPI network (*Figure 2C*). miRanda and TargetScan were used to predict the target genes of *miR-940* and carry out GO and KEGG pathway analyses. GO analysis showed that the assembly functions of targets regulated by *miR-940* were mainly enriched in biological processes, such as cell cycle G1/S phase transition, regulation of myeloid cell differentiation, G1/S transition of mitotic cell cycle, response to light stimulus, cellular response to abiotic stimulus, cellular response to environmental stimulus, and neuron death (*Figure 2D*). KEGG pathway analysis showed that the signal transduction pathway of *miR-940* target assembly was enriched in the transcriptional misregulation in cancer, human cytomegalovirus infection, cortisol synthesis

and secretion, transforming growth factor-beta (TGF-beta) signaling pathway, parathyroid hormone synthesis, secretion and action, tumor necrosis factor (TNF) signaling pathway, and estrogen signaling pathway (*Figure 2E*).

The relative expression of qRT-PCR detection of *miR-940* in the high-risk group ($n=8$) was lower than that in the low-risk group ($n=8$), which was consistent with the results of array analysis, and the difference was statistically significant ($P=0.0324$; *Figure 3A*). The clinical characters of these 16 patients are shown in *Table S1*. The cell numbers in the circular area of the cell culture pore are shown in *Figure 3B*, which shows the radius 0.96 μm away from the central point. The number of lung adenocarcinoma cells (A549) was significantly decreased after *miR-940* was transfected in the cell lines (45 vs. 135; $P<0.0001$; *Figure 3C*). Ten EMT-associated genes [*MMP9* (matrix metalloproteinase 9), *ZEB1* (zinc finger E-box binding homeobox 1), *CDH1* (cadherin 1), *KRT8* (keratin 8), *KRT18* (keratin 18), *KRT19* (keratin 19), *TWIST1* (twist basic helix-loop-helix transcription factor 1), *VIM* (vimentin), *SNAIL1* (snail family zinc finger 1), and *SNAIL2* (snail family zinc finger 2)] were found to be significantly related to the *miR-940* from the cell function experiment ($P<0.05$; *Figure 3D*).

Cell cycle analysis showed that the percentage of cells in G1 phase, S phase, and G2/M phase had no significant differences after transfection of *miR-940* into lung adenocarcinoma A-549 cells (*Figure S2A*). The expression

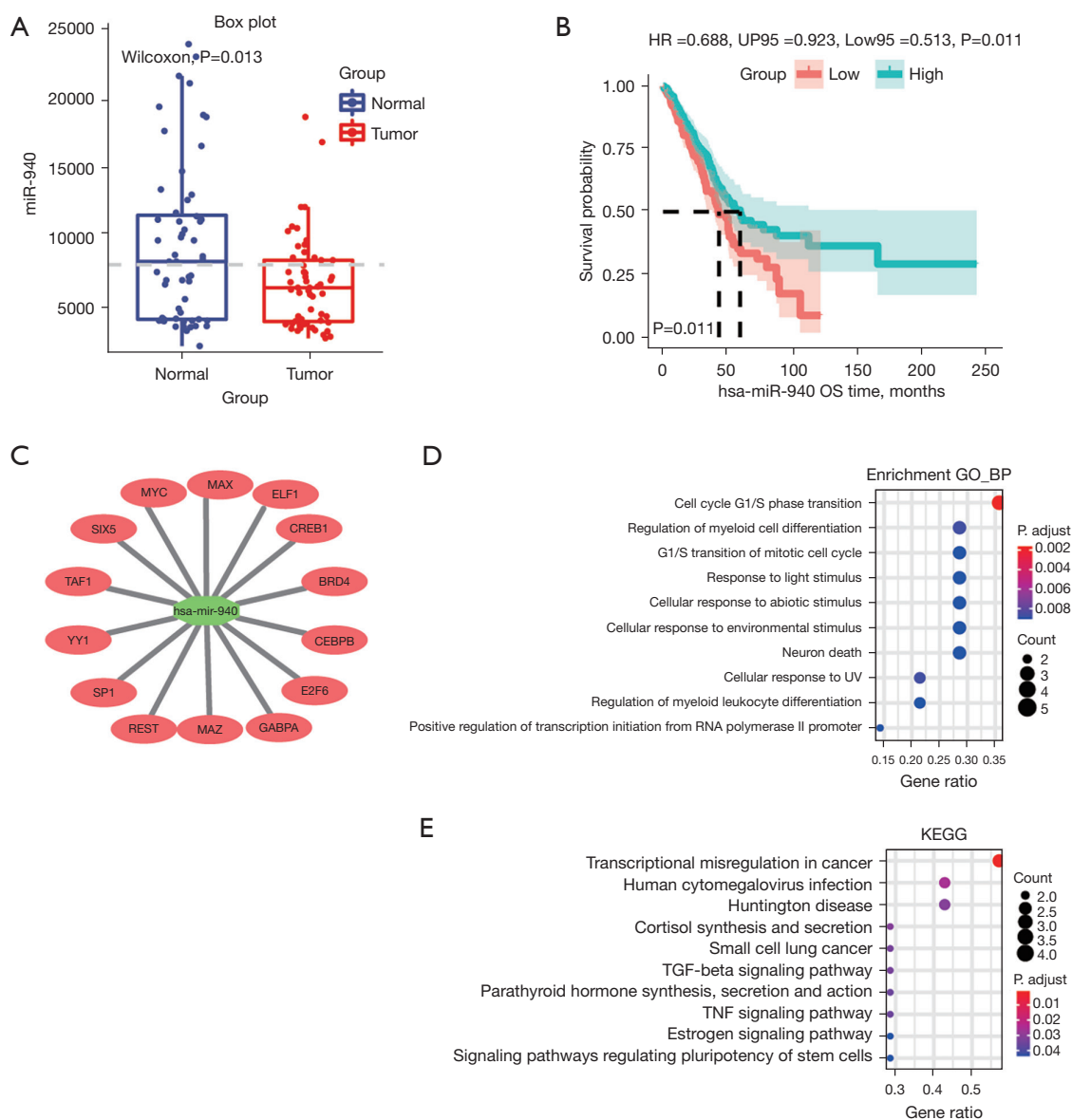


Figure 2 Bioinformatic analysis of miR-940 based on the public database. (A) The differential expression of *miR-940* was analyzed by using the Gene Expression Omnibus (GEO) data from GSE 36681. The expression level of *miR-940* in the tumor group (n=56) was lower than that in normal tissue (n=56; P=0.013). (B) The overall survival rate in the high expression *miR-940* group (n=253) was significantly higher than that in the with low *miR-940* expression (n=252) group in TCGA data (HR =0.688; P=0.011). (C) Fourteen upregulated genes [*MYC* (myelocytomatosis), *MAX*, *ELF1* (E74 like ETS transcription factor 1), *CREB1* (cAMP responsive element binding protein 1), *BRD4* (bromodomain containing 4), *CEBPB* (CCAAT/enhancer binding protein (C/EBP), beta), *E2F6* (E2F transcription factor 6), *GABPA* (GA repeat binding protein, alpha), *MAZ* (MYC-associated zinc finger protein), *REST* (RE1-silencing transcription factor), *SP1* (trans-acting transcription factor 1), *YY1* (YY1 transcription factor), *TAF1* (TATA-box binding protein associated factor 1), *SIX5* (sine oculis-related homeobox 5)] were found to be interactional in the PPI network. (D) Gene Ontology (GO) analysis: the assembly functions of targets regulated by *miR-940* were mainly enriched in cell cycle G1/S phase transition, regulation of myeloid cell differentiation, G1/S transition of mitotic cell cycle, response to light stimulus, cellular response to abiotic stimulus, cellular response to environmental stimulus, and neuron death. (E) Kyoto Encyclopedia of Genes and Genomes (KEGG) Pathway analysis: The signal transduction pathway of *miR-940* target assembly was enriched in the transcriptional misregulation in cancer; human cytomegalovirus infection; cortisol synthesis and secretion; TGF-beta signaling pathway; parathyroid hormone synthesis, secretion, and action; tumor necrosis factor (TNF) signaling pathway; and estrogen signaling pathway.

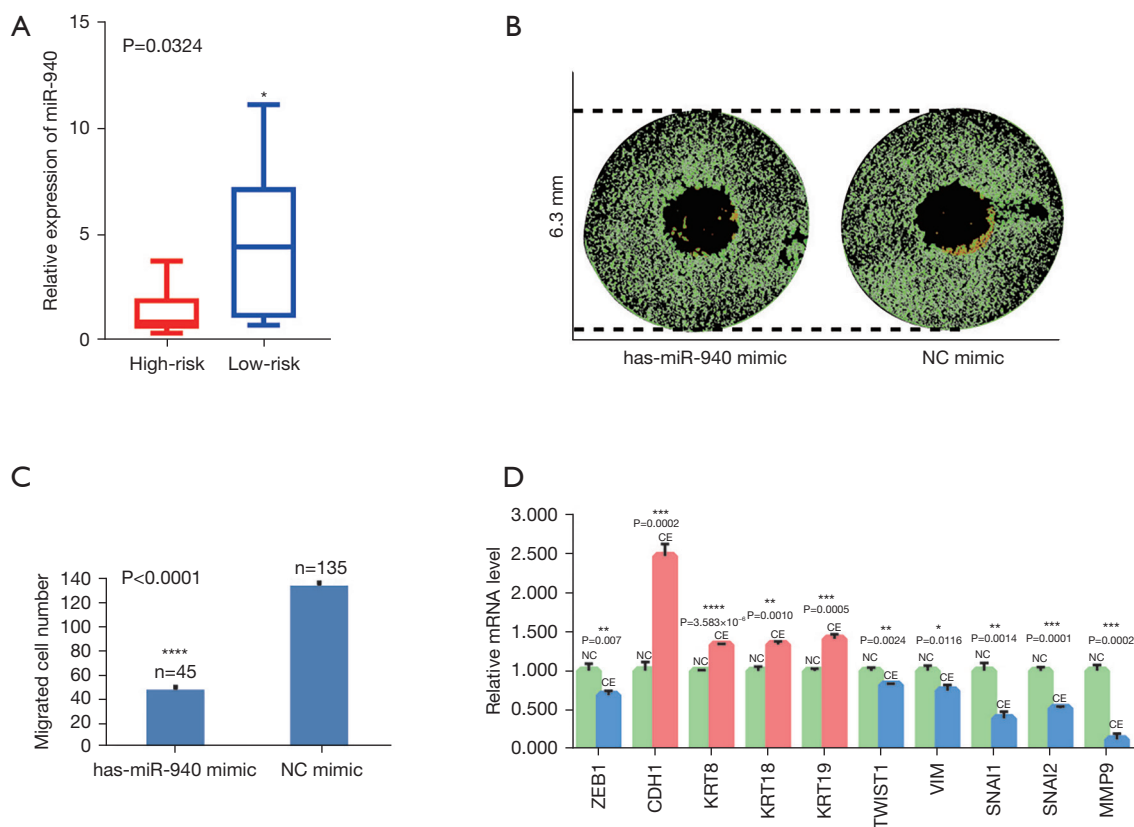


Figure 3 qRT-PCR validation of the expression of *miR-940* from the tissue sample and cell function experiment of the lung adenocarcinoma cell A-549. (A) The relative expression of qRT-PCR detection of *miR-940* in the high-risk group (n=8) was lower than of the low-risk group (n=8), and the difference was statistically significant (P=0.0324). (B) The pictures of the cell numbers in the circular area of the cell culture pore. The radius is 0.96 μ m away from the central point. These intensive experiments were done on the Acumen eX3 platform, which is based on laser scanning imaging. The stain method is DAPI [2-(4-Amidinophenyl)-6-indolecarbamide dihydrochloride]. (C) The number of lung adenocarcinoma cells (A549) was significantly decreased after *miR-940* was transfected in the cell lines (45 vs. 135; P<0.0001). (D) Ten EMT-associated genes [*MMP9* (matrix metalloproteinase 9), *ZEB1* (zinc finger E-box binding homeobox 1), *CDH1* (cadherin 1), *KRT8* (keratin 8), *KRT18* (keratin 18), *KRT19* (keratin 19), *TWIST1* (twist basic helix-loop-helix transcription factor 1), *VIM* (vimentin), *SNAI1* (snail family zinc finger 1), and *SNAI2* (snail family zinc finger 2)] were found to significantly related to the *miR-940* from the cell function experiment. *, P<0.05; **, P<0.01; ***, P<0.001; ****, P<0.0001.

level of *MMP9* in lung adenocarcinoma tumor tissue (n=483) was higher than that in the normal tissue (n=347; P<0.05; Figure S2B). In the Kaplan-Meier plotter survival analysis, the low-*MMP9* expression group (n=102) had better survival rates than did the high-*MMP9* expression group (n=101) especially for stage I female lung adenocarcinoma patients (Figure S2C). The risk factor was 1.86 (1.06–3.24; P=0.027).

Discussion

Goodgame *et al.* (6) studied the prognosis of 715 patients

with NSCLC who underwent surgery and reported that the 5-year survival rate of stage I patients was 66%, with 19% having tumor metastases occurring within 5 years. Detterbeck *et al.* (7) reported that 73% of patients with stage I lung cancer had a satisfactory prognosis in the low-risk group, 27% of patients still had a poor prognosis, and most patients in the high-risk group died due to postoperative tumor recurrence or metastasis.

The miRNAs to be validated were mostly selected through the combination of literature support and P value. Three miRNAs were locked out of 24 differential miRNAs. Compared with the other two miRNAs, *miR-*

940 has been supported by relevant literature to play a role in tumor metastasis, but has not been thoroughly studied in lung adenocarcinoma. *miR-940* was reported to have tumor inhibition impacts in many types of tumor, such as glioblastoma (26) and hepatocellular carcinoma (27). Our study revealed that *miR-940* was downregulated in the high-risk nonsmoking female stage I lung adenocarcinoma patients compared with the control group. Meanwhile, the expression level of *miR-940* was associated with better survival for early stage lung adenocarcinoma patients. After that, functional experiments further suggested that upregulation of *miR-940* impeded cell growth, migration, and the EMT of lung adenocarcinoma cells *in vivo*.

In terms of mechanism, Gu *et al.* reported that *miR-940* could mediate family sequence similarity 83 member F (*FAM83F*) expression, consequently repressing the NSCLC cell proliferation (17). Jiang *et al.* demonstrated that *miR-940* could inhibit cell invasion by targeting *Snail* in NSCLC (18). In addition, Huang *et al.* reported that circ_0000735 modulated *miR-940* to regulate *BMPER* expression (28). Indeed, this axis plays an important role in NSCLC progression. Ten EMT-associated genes (*MMP9*, *ZEB1*, *CDH1*, *KRT8*, *KET19*, *TWIST1*, *VIM*, *SNAI1*, and *SNAI2*) were found to be significantly related to *miR-940* in the cell function experiment. And the results of *MMP9* have the most significant value. Based on the Kaplan-Meier plotter method, we speculated that matrix metalloproteinase 9 (*MMP9*) was the functional target of *miR-940*. The expression level of *MMP9* in lung adenocarcinoma tumor tissue was higher than that in normal tissue. Furthermore, the low *MMP9* expression group had better survival rates especially for stage I female lung adenocarcinoma patients. MMPs were a diverse group of molecular markers for prognosis and prediction of lung cancer. A high level of *MMP9* expression has been significantly correlated with poor survival of surgical patients (29,30). Furthermore, *MMP9* was found to be correlated with lung adenocarcinoma's different pathological subtypes. *MMP9* activity was the highest in solid-predominant and micropapillary-predominant subtypes, intermediate in the acinar-predominant and papillary-predominant subtypes, and the lowest in the lepidic-predominant subtype. *MMP9* was identified as a valuable biological target for the early diagnosis and targeted therapy of lung cancer. Moreover, the level of *MMP9* expression was also correlated with cancer classification and OS of breast cancer (31), gastric cancer (32), and prostate cancer (33).

Further investigation is required to understand the

expression and biological function of *miR-940* within lung adenocarcinoma. GO analysis showed that the assembly functions of targets regulated by *miR-940* were mainly enriched in biological processes, such as cell cycle G1/S phase transition, regulation of myeloid cell differentiation, G1/S transition of mitotic cell cycle, response to light stimulus, cellular response to abiotic stimulus, cellular response to environmental stimulus, and neuron death. KEGG pathway analysis showed that the signal transduction pathway of *miR-940* target assembly was enriched in the transcriptional misregulation in cancer; human cytomegalovirus infection; cortisol synthesis and secretion; TGF-beta signaling pathway; parathyroid hormone synthesis, secretion and action; TNF signaling pathway; and estrogen signaling pathway. Jiang *et al.* reported that *miR-940* inhibits TGF-beta-induced EMT and cell invasion by targeting *Snail* in NSCLC. Overexpression of *miR-940* significantly inhibited *Snail* mRNA and protein expression in A549 and H226 cells (18). Meanwhile, Wang *et al.* observed that *miR-940* indirectly upregulated programmed cell death-1 (*PD-L1*) through inhibition of Casitas B-lineage lymphoma-b (*Cbl-b*) and Casitas B-lineage lymphoma-c (*Cbl-c*) and induction of the *STAT3/AKT/ERK* signaling in wild-type epidermal growth factor receptor (*EGFR*) cell lines (34). Cao *et al.* explored the potential role of *miR-940* in the regulation of immune response. They found that pathogenesis of osteoarthritis can be regulated by the *miR-940-MyD88* axis, which can be achieved through the combined signaling mechanism of *MyD88-NF-κB* signaling, induced with the help of interleukin-1β (35). Similarly, Song *et al.* reported that a low level of *miR-940* and a high level of *MyD88* in pancreatic ductal adenocarcinoma (PDAC) promoted PDAC cell growth which might be related to the low survival rate of PDAC patients. *miR-940* exerted its effect by targeting *MyD88* (36). Wang *et al.* found that upregulation of *miR-940* may function as a suppressor in the progression of ovarian cancer by inhibiting cell proliferation and inducing apoptosis by targeting *PKC-δ* (37). Jiang *et al.* found that *miR-940* expression was negatively correlated with NSCLC metastasis and clinical stages. They confirmed a targeted inhibition for *Snail* expression from *miR-940*. Meanwhile, they found that overexpression of *miR-940* obstructed TGF-β-induced EMT and cell migration and invasion in NSCLC cells (18). Our findings suggest that *miR-940* may participate in the regulation of the TGF-beta and TNF signaling pathway and thus lead to prognostic stratification of nonsmoking female patients with stage I lung adenocarcinoma.

Strengths is that miR-940 might be a protective factor for positive prognosis in early stage nonsmoking female lung adenocarcinoma, This might be a clue for a new treatment target. The main limitation of the present study is that a relatively small number of patients were involved in the analysis. Further studies are thus essential to investigating the regulation of *MMP9*, TGF-beta, and TNF signaling pathways by *miR-940*.

Conclusions

Our findings clarified the role of *miR-940* and enriched the data concerning lung adenocarcinoma diagnosis. *miR-940* was closely associated with lung adenocarcinoma development. *miR-940* might be a protective factor for positive prognosis in early-stage nonsmoking female lung adenocarcinoma, with TGF-beta pathway, TNF pathway, and *MMP9* being the potential targets. This might be helpful in developing potential targets in lung adenocarcinoma diagnosis and therapies.

Acknowledgments

The authors appreciate the academic support from the AME Lung Cancer Collaborative Group. The authors also appreciate the great support from Dr. Kwun M. Fong (The Prince Charles Hospital, Australia) in improving the quality of this paper.

Funding: This study was supported by funding from the China-Japan Friendship Hospital (No. 2015-1-QN-20), Overseas Scholarship (No. 2014-QTL-032), Peking science and technology fund (No. Z191100006619008), and Elite Medical Professionals project of China-Japan Friendship Hospital (No. ZRJY2021-GG02).

Footnote

Reporting Checklist: The authors have completed the REMARK reporting checklist. Available at <https://dx.doi.org/10.21037/tlcr-21-906>

Data Sharing Statement: Available at <https://dx.doi.org/10.21037/tlcr-21-906>

Conflicts of Interest: All authors have completed the ICMJE uniform disclosure form (available at <https://dx.doi.org/10.21037/tlcr-21-906>). The authors have no conflicts of interest to declare.

Ethical Statement: The authors are accountable for all aspects of the work in ensuring that questions related to the accuracy or integrity of any part of the work are appropriately investigated and resolved. All procedures performed in this study involving human participants were in accordance with the Declaration of Helsinki (as revised in 2013). The study was approved by ethics board of China-Japan Friendship Hospital (No. 2020-116-K75) and informed consent was taken from all the patients.

Open Access Statement: This is an Open Access article distributed in accordance with the Creative Commons Attribution-NonCommercial-NoDerivs 4.0 International License (CC BY-NC-ND 4.0), which permits the non-commercial replication and distribution of the article with the strict proviso that no changes or edits are made and the original work is properly cited (including links to both the formal publication through the relevant DOI and the license). See: <https://creativecommons.org/licenses/by-nc-nd/4.0/>.

References

1. Siegel RL, Miller KD, Jemal A. Cancer statistics, 2015. *CA Cancer J Clin* 2015;65:5-29.
2. DeSantis CE, Lin CC, Mariotto AB, et al. Cancer treatment and survivorship statistics, 2014. *CA Cancer J Clin* 2014;64:252-71.
3. Sher T, Dy GK, Adjei AA. Small cell lung cancer. *Mayo Clin Proc* 2008;83:355-67.
4. Burgess TL, Sun J, Meyer S, et al. Biochemical characterization of AMG 102: a neutralizing, fully human monoclonal antibody to human and nonhuman primate hepatocyte growth factor. *Mol Cancer Ther* 2010;9:400-9.
5. Tang W, Lei Y, Su J, et al. TNM stages inversely correlate with the age at diagnosis in ALK-positive lung cancer. *Transl Lung Cancer Res* 2019;8:144-54.
6. Goodgame B, Viswanathan A, Miller CR, et al. A clinical model to estimate recurrence risk in resected stage I non-small cell lung cancer. *Am J Clin Oncol* 2008;31:22-8.
7. Detterbeck FC, Boffa DJ, Tanoue LT. The new lung cancer staging system. *Chest* 2009;136:260-71.
8. Bartel DP. MicroRNAs: genomics, biogenesis, mechanism, and function. *Cell* 2004;116:281-97.
9. Friedman RC, Farh KK, Burge CB, et al. Most mammalian mRNAs are conserved targets of microRNAs. *Genome Res* 2009;19:92-105.
10. Mitchell PS, Parkin RK, Kroh EM, et al. Circulating microRNAs as stable blood-based markers for cancer

- detection. *Proc Natl Acad Sci U S A* 2008;105:10513-8.
11. Jeong HC, Kim EK, Lee JH, et al. Aberrant expression of let-7a miRNA in the blood of non-small cell lung cancer patients. *Mol Med Rep* 2011;4:383-7.
 12. Chen X, Ba Y, Ma L, et al. Characterization of microRNAs in serum: a novel class of biomarkers for diagnosis of cancer and other diseases. *Cell Res* 2008;18:997-1006.
 13. Landi MT, Zhao Y, Rotunno M, et al. MicroRNA expression differentiates histology and predicts survival of lung cancer. *Clin Cancer Res* 2010;16:430-41.
 14. Bishop JA, Benjamin H, Cholak H, et al. Accurate classification of non-small cell lung carcinoma using a novel microRNA-based approach. *Clin Cancer Res* 2010;16:610-9.
 15. Liu W, Xu Y, Guan H, et al. Clinical potential of miR-940 as a diagnostic and prognostic biomarker in breast cancer patients. *Cancer Biomark* 2018;22:487-93.
 16. Hu J, Li C, Liu C, et al. Expressions of miRNAs in papillary thyroid carcinoma and their associations with the clinical characteristics of PTC. *Cancer Biomark* 2017;18:87-94.
 17. Gu GM, Zhan YY, Abuduwaili K, et al. MiR-940 inhibits the progression of NSCLC by targeting FAM83F. *Eur Rev Med Pharmacol Sci* 2018;22:5964-71.
 18. Jiang K, Zhao T, Shen M, et al. MiR-940 inhibits TGF- β -induced epithelial-mesenchymal transition and cell invasion by targeting Snail in non-small cell lung cancer. *J Cancer* 2019;10:2735-44.
 19. Betel D, Koppal A, Agius P, et al. Comprehensive modeling of microRNA targets predicts functional non-conserved and non-canonical sites. *Genome Biol* 2010;11:R90.
 20. Ashburner M, Ball CA, Blake JA, et al. Gene ontology: tool for the unification of biology. The Gene Ontology Consortium. *Nat Genet* 2000;25:25-9.
 21. Gene Ontology Consortium. The Gene Ontology (GO) project in 2006. *Nucleic Acids Res* 2006;34:D322-6.
 22. Draghici S, Khatri P, Tarca AL, et al. A systems biology approach for pathway level analysis. *Genome Res* 2007;17:1537-45.
 23. Yi M, Horton JD, Cohen JC, et al. WholePathwayScope: a comprehensive pathway-based analysis tool for high-throughput data. *BMC Bioinformatics* 2006;7:30.
 24. Rao X, Huang X, Zhou Z, et al. An improvement of the $2^{-\Delta\Delta CT}$ method for quantitative real-time polymerase chain reaction data analysis. *Biostat Bioinforma Biomath* 2013;3:71-85.
 25. Wright GW, Simon RM. A random variance model for detection of differential gene expression in small microarray experiments. *Bioinformatics* 2003;19:2448-55.
 26. Luo H, Xu R, Chen B, et al. MicroRNA-940 inhibits glioma cells proliferation and cell cycle progression by targeting CKS1. *Am J Transl Res* 2019;11:4851-65.
 27. Li P, Xiao Z, Luo J, et al. MiR-139-5p, miR-940 and miR-193a-5p inhibit the growth of hepatocellular carcinoma by targeting SPOCK1. *J Cell Mol Med* 2019;23:2475-88.
 28. Huang W, Xu X, Liu M, et al. Downregulation of Hsa_circ_0000735 Inhibits the Proliferation, Migration, Invasion, and Glycolysis in Non-small-cell Lung Cancer by Targeting miR-940/BMPER Axis. *Onco Targets Ther* 2020;13:8427-39.
 29. Liu J, Ping W, Zu Y, et al. Correlations of lysyl oxidase with MMP2/MMP9 expression and its prognostic value in non-small cell lung cancer. *Int J Clin Exp Pathol* 2014;7:6040-7.
 30. Jian H, Zhao Y, Liu B, et al. SEMA4b inhibits MMP9 to prevent metastasis of non-small cell lung cancer. *Tumour Biol* 2014;35:11051-6.
 31. Yousef EM, Tahir MR, St-Pierre Y, et al. MMP-9 expression varies according to molecular subtypes of breast cancer. *BMC Cancer* 2014;14:609.
 32. Kuang RG, Wu HX, Hao GX, et al. Expression and significance of IGF-2, PCNA, MMP-7, and α -actin in gastric carcinoma with Lauren classification. *Turk J Gastroenterol* 2013;24:99-108.
 33. Yamaguchi NH, Lichtenfels AJ, Demarchi LM, et al. COX-2, MMP-9, and Noguchi classification provide additional prognostic information about adenocarcinoma of the lung. A study of 117 patients from Brazil. *Am J Clin Pathol* 2004;121:78-86.
 34. Wang S, Xu L, Che X, et al. E3 ubiquitin ligases Cbl-b and c-Cbl downregulate PD-L1 in EGFR wild-type non-small cell lung cancer. *FEBS Lett* 2018;592:621-30.
 35. Cao J, Liu Z, Zhang L, et al. miR-940 regulates the inflammatory response of chondrocytes by targeting MyD88 in osteoarthritis. *Mol Cell Biochem* 2019;461:183-93.
 36. Song B, Zhang C, Li G, et al. MiR-940 inhibited pancreatic ductal adenocarcinoma growth by targeting MyD88. *Cell Physiol Biochem* 2015;35:1167-77.
 37. Wang F, Wang Z, Gu X, et al. miR-940 Upregulation Suppresses Cell Proliferation and Induces Apoptosis by Targeting PKC- δ in Ovarian Cancer OVCAR3 Cells. *Oncol Res* 2017;25:107-14.

Cite this article as: Ma Q, Zhang J, Huang J, Wang X, Xiao F, Xing H, Wang Y, Guo Y, Shi B, Song Z, Liu D, Si C, Horinouchi H, Liang C. Decreased *miR-940* expression can predict a negative prognosis in early-stage nonsmoking female lung adenocarcinoma. *Transl Lung Cancer Res* 2021;10(11):4293-4302. doi: 10.21037/tlcr-21-906

Table S1 Clinical pathological characters of the 16 patients for *miRNA-940* qRT-PCR validation

Group	Age	Gender	Smoke	Size (cm)	Invasive	Subtypes (%)					Stage
						L	A	P	MP	S	
B1	61	F	N	2.5	–	15	70	10	5	0	IA
B2	70	F	N	4.0	PI+	0	30	0	60	10	IB
B3	54	F	N	2.5	PI+	10	90	0	0	0	IB
B4	56	F	N	1.7	PI+	50	40	10	0	0	IB
B5	74	F	N	2.5	–	0	15	80	5	0	IA
B6	58	F	N	2.5	PI+	5	40	55	0	0	IB
B7	68	F	N	3.0	–	0	15	80	5	0	IA
B8	66	F	N	2.5	–	0	90	0	0	10	IA
A1	63	F	N	1.5	–	10	90	0	0	0	IA
A2	73	F	N	2.2	–	20	80	0	0	0	IA
A3	67	F	N	1.7	PI+	10	80	10	0	0	IB
A4	45	F	N	3.0	–	0	75	0	5	20	IA
A5	48	F	N	0.8	–	20	80	0	0	0	IA
A6	67	F	N	1.5	–	80	20	0	0	0	IA
A7	64	F	N	2.0	–	10	80	10	0	0	IA
A8	62	F	N	1.8	PI+	30	70	0	0	0	IB

B1–B6: high-risk group; A1–A6. F, female; N, none; cm, centimeter; PI+, pleural invasion; V+, vessel invasion; L, lepidic subtype; A, acinar subtype; P, papillary subtype; MP, micropapillary subtype; S, solid subtype.

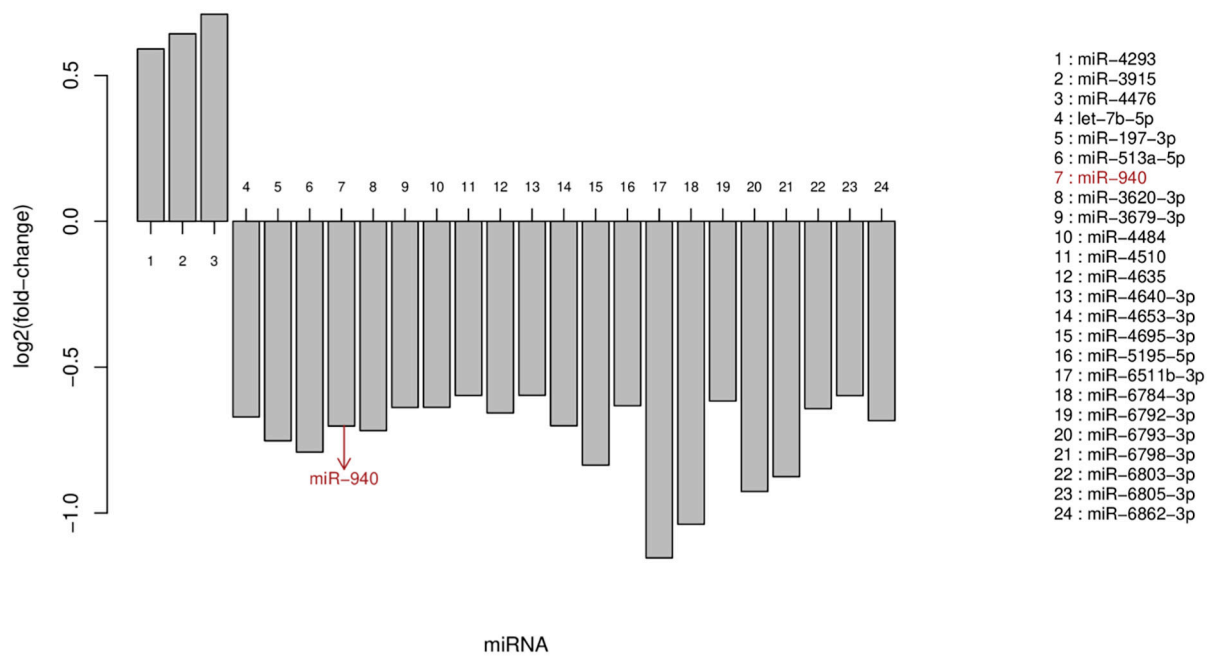


Figure S1 miRNA expression profile from the comparison of the high-risk and low-risk group. The results of the miRNA expression profile were analyzed by *t*-test using the RVM based on a small sample, of which 24 kinds of miRNAs were selectively screened. Low expression was found in 3 kinds of miRNAs (*miR-4293*, *miR-3915*, and *miR-4476*), and high expression was found in 21 kinds of miRNAs (*let-7b-5p*, *miR-197-3p*, *miR-513a-5p*, *miR-940*, *miR-3620-3p*, *miR-3679-3p*, *miR-4484*, *miR-4510*, *miR-4635*, *miR-4640-3p*, *miR-4653-3p*, *miR-4695-3p*, *miR-5195-5p*, *miR-6511b-3p*, *hsa-miR-6784-3p*, *miR-6792-3p*, *miR-6793-3p*, *miR-6798-3p*, *miR-6803-3p*, *miR-6805-3p*, and *miR-6862-3p*; $P < 0.05$; FDR < 0.05).

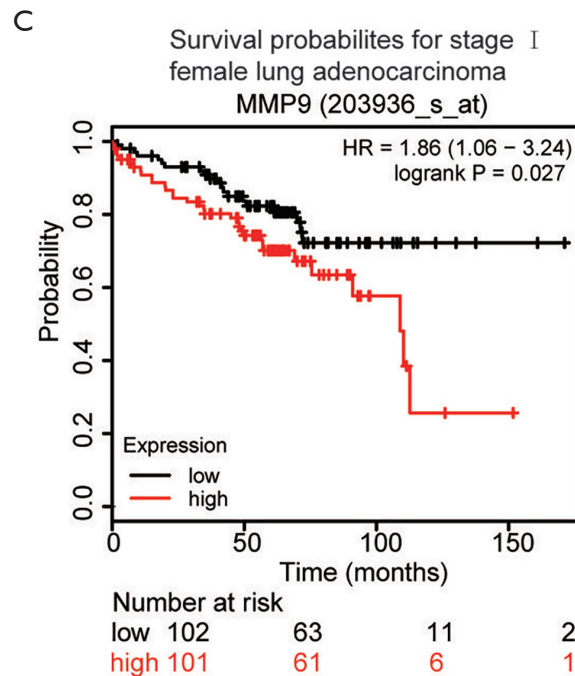
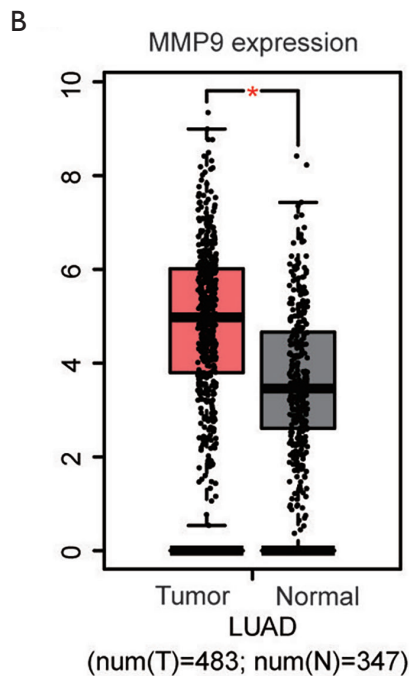
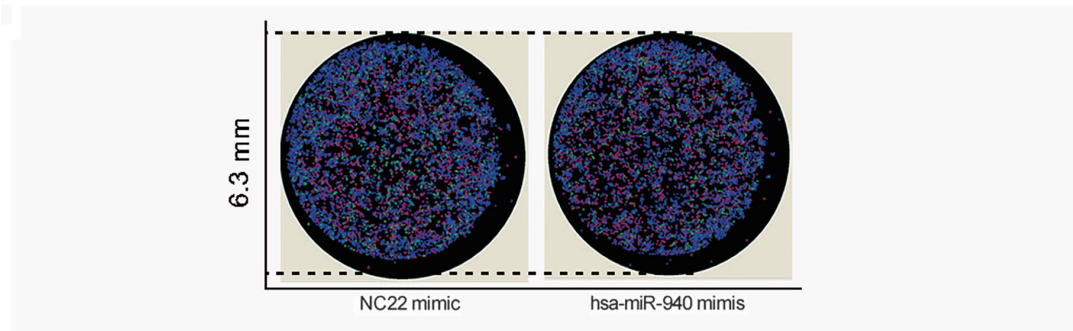
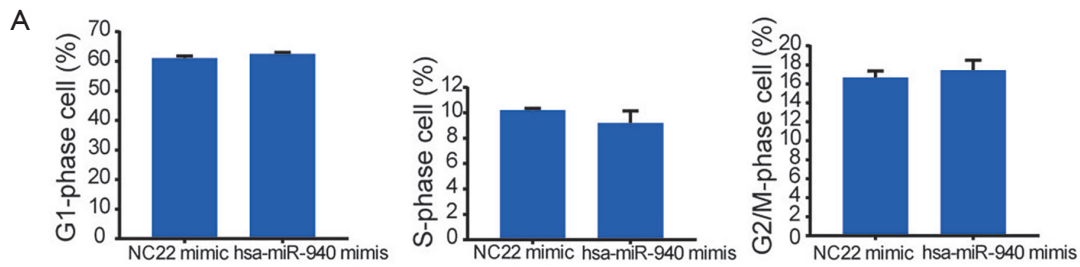


Figure S2 Cell cycle analysis and the relationship between *miR-940* and matrix metalloproteinase 9 (*MMP9*). (A) Cell cycle analysis showed that the percentage of cells in G1 phase, S phase, and G2/M phase had no significant difference after transfection of *miR-940* into the lung adenocarcinoma A-549 cells. These intensive experiments were done on the Acumen eX3 platform, which is based on laser scanning imaging. The stain method is DAPI [2-(4-Amidinophenyl)-6-indolecarbamidine dihydrochloride]. (B) The expression level of *MMP9* in LUAD tumor tissue (n=483) was higher than that in normal tissue (n=347; P<0.05) (*, P<0.05). (C) In the Kaplan-Meier plotter survival analysis, the low *MMP9* expression group (n=102) had better survival rates than did the high *MMP9* expression group (n=101), especially for stage I female LUAD patients. The risk factor was 1.86 (1.06–3.24; P=0.027).